COBEM 2023 27TH INTERNATIONAL CONGRESS OF MECHANICAL ENGENEERING

ABCM Brazilian Society of Mechanical Sciences and Engineering
27th ABCM International Congress of Mechanical Engineering
December 04-08, 2023, Florianópolis-SC, Brazil

VORTEX-INDUCED MOTION OF A MULTICOLUMN FLOATING OFFSHORE WIND TURBINE PLATFORM: A STUDY COMPARING TWO MODELLING APPROACHES – CFD AND A REDUCED ORDER MODEL

André X. Scopel[1]
Éverton L. de Oliveira[2]
[1]Centre of Dynamics and Fluids (NDF)
[2]Offshore Mechanics Laboratory (LMO)
Escola Politécnica (POLI), University of São Paulo (USP)
andrexscopel@usp.br, ev_lins@usp.br

Bruno S. Carmo[1]
bruno.carmo@usp.br

Celso P. Pesce[2]
ceppesce@usp.br

Abstract. *The aim of this paper is to model the hydrodynamic behavior of a moored FOWT – Floating Offshore Wind Turbine platform - under a constant current flow, considering the motions in the horizontal plane only. The investigated floating unity is a 4-columned semisubmersible platform with the wind turbine mounted over one of the columns – the central one. Two modelling approaches are compared to experimental data, obtained with a small-scale model, to access their validity, advantages, disadvantages, and usage. The first approach, the ROM, considers the hydrodynamic forces caused by the current represented with phenomenological models - wake oscillators based on forced van der Pol equations, in which the adopted Strouhal numbers consider the aspect ratio of the columns. The CFD approach considers a time-dependent two-dimensional model, employing finite volume discretization applied to a URANS formulation which uses the k-omega SST turbulence closure model. The numerical model is built considering the platform as a rigid body and using a deformable mesh. Both approaches are calculated assuming average Reynolds numbers between 8000 and 70000, in the small model scale, and reduced velocities between 3 and 24. Guided by the experimental tests, the resulting dynamic behaviors are compared, and conclusions are drawn about the efficiency, strengths, and limitations of the proposed approaches, assessing them as potential design tools.*

Keywords: *vortex-induced motions, floating offshore wind turbines, Reduced Order Model, phenomenological models, forced van der Pol equation, computational fluid dynamics (CFD), URANS, small scale experiments.*

1. INTRODUCTION

Wind turbines are among the most promising technologies in modern engineering and clean power generation. Currently, wind energy represents a significant and increasing share of the total energy generated around the world, particularly in Brazil. In 2022, it represented the third main source of electric energy, providing around 10% of the national electric annual power (EPE, 2022). While most of the installed capacity in the world is on land, an increasing number of installations has been taking place offshore. A wind turbine in the sea can be either on a platform fixed at the bottom of the ocean or on a floating platform. Typically, beyond 60 m the use of fixed platforms becomes impracticable, and the use of floating offshore wind turbines (FOWTS) becomes a feasible alternative. However, the floating platform motions caused by the action of current, waves and wind may impair the efficiency of the turbine. Particularly, it is important to understand the hydrodynamics of the system and predict the forces and displacements imposed by the ocean environment loads. This paper focuses on the vortex-induced motions (VIM) problem of a semisubmersible wind turbine platform subjected to constant current.

The VIM is a fluid-structure interaction phenomena caused by periodic vortex emissions downstream from a body immersed in a flow. The vortex shedding changes the pressure field around the body and can cause it to oscillate and interact with the flow in a complex and non-linear manner. If one of the natural frequencies of the system is stimulated by the dominant wake frequency, we can observe a synchronization phenomenon between the vortex shedding and the system natural frequencies, known as lock-in, resulting in an increase of movement amplitudes, which can be detrimental to the wind turbine's performance as well to the mooring system.

This study compares and assesses two different modelling approaches for this phenomenon by comparing the results with small-scale model experimental data obtained by (Gonçalves, et al., 2019). The CFD method is one logical choice of VIM modelling, as it can resolve the Navier-Stokes equations and predict the velocity and pressure fields around the

body. However, such a technique demands a lot of computational power and requires verification and validation procedures that are not always feasible during first design phases. On the other hand, the reduced order model (ROM), based on wake-oscillators approaches, proposed by (de Oliveira, Pesce, Mendes, Orsino, & Franzini, 2020) is an alternative that provides faster and more scalable simulations. The methods are herein sued to simulate the VIM of the OC4 semi-submersible floating offshore wind turbine (FOW), at a small experimental scale (1:72.72, as presented by (Gonçalves, et al., 2019). Both techniques are applied by restricting the moored FOWT dynamics on the horizontal plane, under two-dimensional flow hypotheses. Preliminary results are compared and discussed, having the experimental data in the background, upon which further work are suggested.

2. MODELING

The simulations were performed using the OC4 semisubmersible platform, considering a scaling of 1:72.72 (Gonçalves, et al., 2019). The geometry and main dimensions of the scale model are presented in Figure 1. The simulations considered only the external and the central columns in only one incidence angle, namely 0º, as shown in Figure 2.

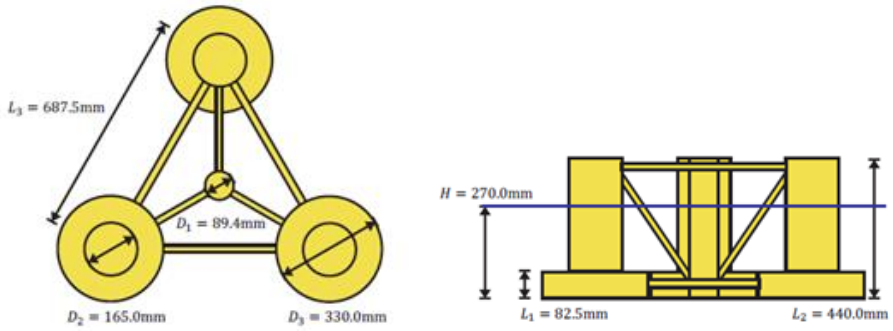

Figure 1. OC4 platform geometry, model scale (1:72.72) dimensions. Adapted from Gonçalves et al. (2019).

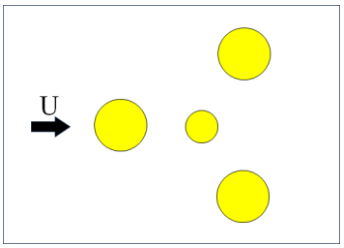

Figure 2. OC4 simplified geometry and the three incidence angles used in the simulations.

As is commonly made in VIV/VIM studies, the results are explored and presented in terms of reduced velocities,

$$V_r = \frac{UT_{0,Y}}{D}, \tag{1}$$

which is a non-dimensional number that relates the incoming flow velocity, U, with the natural period of motion in the transverse direction, $T_{0,Y}$, and the characteristic length of the body, D, here taken as the diameter of the three main columns.

The results are compared by taking nondimensional harmonic-equivalent amplitudes of the motions in-line (X) and transverse (Y) to the current and of the rotational motion (ψ) on the horizontal plane[1],

$$A_{x,y} = \frac{\sqrt{2}\sigma_{x,y}}{D}; \quad A_{yaw} = \sqrt{2}\sigma_{\psi}, \tag{2}$$

where σ represents the corresponding standard deviations from the mean. The hydrodynamic forces aligned with and transverse to the flow, $F_{HX}(t)$ and $F_{HY}(t)$, are represented by the non-dimensional drag and lift coefficients,

[1] For conciseness, herein named *surge*, *sway* and *yaw* motions, respectively.

$$C_{D,\,\mathrm{MEAN}} = \frac{\bar{F}_{HX}(t)}{\frac{1}{2}\rho A_p U^2}; \quad C_{D,\,\mathrm{RMS}} = \frac{\sigma_{F_{HX}}(t)}{\frac{1}{2}\rho A_p U^2}; \quad C_{L,\,\mathrm{RMS}} = \frac{\sigma_{F_{HX}}(t)}{\frac{1}{2}\rho A_p U^2}, \tag{3}$$

in which,

$$A_p = 3\left(D_2\left(H - L_1\right) + D_3 L_1\right). \tag{4}$$

is the projected area, perpendicular to the incoming flow, adopted by (Gonçalves, et al., 2019); see Figure 1.

2.1 CFD

The computational fluid dynamics (CFD) simulations were performed in a 2-dimensional domain, using the finite volume method provided by the open-source software OpenFOAM (Weller, Tabor, Jasak, & Fureby, 1998). The URANS model was selected for its good cost-benefit relation, as it can provide reliable results while maintaining a feasible computational cost. The turbulence model selected was the *k*-omega SST (Menter, 1994), for its ability to deal with adverse pressure gradients in external flows.

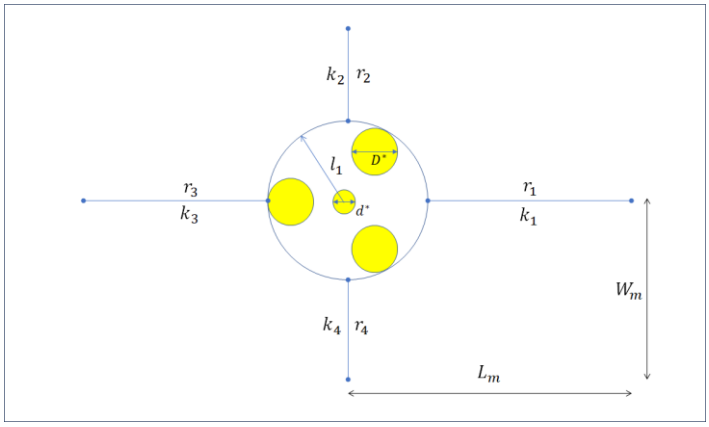

Figure 3. CFD simulation, geometric configuration, and spring distribution.

To represent VIM conditions, the platform was considered a single rigid body, attached to springs that simulate the experimental conditions representing the mooring system on the real platform.

Figure 3 shows the setup. It was implemented through OpenFOAM's sixDoFRigidBodyMotion solver, alongside the dynamicMotionSolverFvMesh. The advantage of these modules is the direct implementation of the springs onto the domain, so the setup configuration becomes quite straightforward. The simulations started from the rest, with the body free to oscillate and subjected to an incoming constant flow velocity.

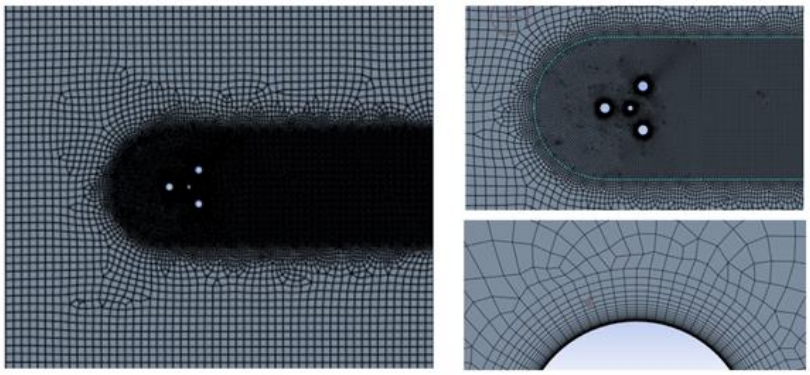

Figure 4. CFD mesh.

The mesh is deformable, updated at each timestep. We employed an adaptive time step for the simulations, with the maximum Courant number set to $\mathrm{Co} = 0.75$. The unstructured mesh was developed in the software Ansys Meshing, using quadrilateral 2-dimensional elements, with 2 regions of refinement, plus an inflation layer, as shown in Figure 4.

Convergence analyses were conducted to evaluate, besides the space discretization, the influence of the maximum y^+ and the domain size. The normalized amplitudes (A_x, A_y) and the force coefficients ($C_{d_{mean}}$, $C_{l_{RMS}}$) were used as refinement criteria. The final mesh has 26323 elements, and a domain size of $47x55\ D$. A value of $y^+_{max} = 1.3$ was achieved by setting the thickness of the inflation's first layer to $7x10^{-4}$, with a growth rate of 1.2 and a total of 23 layers.

As usual in CFD simulations, the domain was non-dimensionalized by the main column diameter, D_2, to facilitate the setup configuration for the several reduced velocities. Therefore, all geometric parameters, such as columns diameters, springs attachment point distances and respective undeformed lengths were made dimensionless accordingly. In the CFD simulations, the non-dimensional forms of the spring constants and the moment of inertia are:

$$k^* = \left[\frac{k}{\rho U^2 L}\right]_{\text{Exp}} \quad ; \quad I^* = \left[\frac{I}{\rho D^4 L}\right]_{\text{Exp}} . \tag{5}$$

Table 1. Reduced velocities and corresponding Reynolds numbers considered in the CFD simulations.

V_r	2.91	4.07	5.24	5.82	6.98	8.15	8.73	9.89	11.05	11.64	12.80	13.96	14.55	17.45
Re	8250	11550	14850	16500	19800	23100	24750	28050	31350	33000	36300	39600	41250	49500

2.2 The Reduced Order Model (ROM)

The detailed deduction of the ROM may be seen in (de Oliveira, Pesce, Mendes, Orsino, & Franzini, 2020). The ROM was developed considering the motion of the platform restricted to the horizontal plane. The platform is taken as a rigid body. The ROM is derived from Lagrange's equations, with 3DoF. The hydrodynamic interaction is emulated through a phenomenological model based on wake-oscillators (Franzini & Bunzel, 2018), two for each column, so that the generalized coordinate vector is expanded to 3+2*N* degrees of freedom, being *N* the number of columns. In the present case, *N* = 4, as the smaller diameter column is also considered. All the ROM parameters may be seen in (de Oliveira, Pesce, Mendes, Orsino, & Franzini, 2020), Tables 1-4.

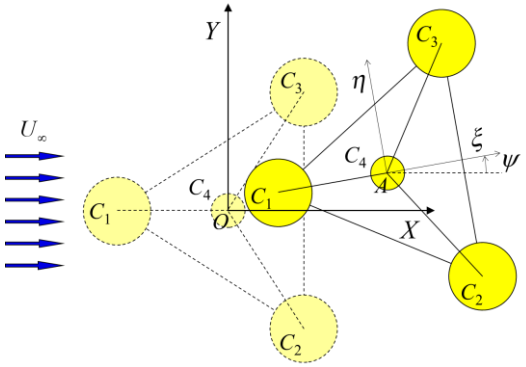

Figure 5. Coordinates and general definitions. At origin, platform is shown at 0 degrees current heading.

Therefore, the resulting 11-dof reduced-order model may be written in the following form:

$$\tilde{\mathbf{M}}\ddot{\tilde{\mathbf{q}}} = \tilde{\mathbf{Q}}_c + \tilde{\mathbf{Q}}_{nc}, \tag{6}$$

where $\tilde{\mathbf{M}}$ and $\tilde{\mathbf{q}}$ are, respectively, the augmented inertia matrix and generalized coordinate vector and, on the r.h.s., $\tilde{\mathbf{Q}}_c$ and $\tilde{\mathbf{Q}}_{nc}$ are, respectively, extended generalized force vectors, the first one dependent on the generalized configuration of the system and the second one on non-conservative terms. Their explicit forms are:

$$\tilde{\mathbf{q}} = \begin{bmatrix} \mathbf{q} \\ \mathbf{w} \end{bmatrix}; \quad \tilde{\mathbf{M}} = \begin{bmatrix} \mathbf{M} & \mathbf{0} \\ \mathbf{A}_w & \mathbf{1} \end{bmatrix}; \quad \tilde{\mathbf{Q}}_c = \begin{bmatrix} \mathbf{Q}^m - \mathbf{Q}^I \\ \mathbf{Q}^r_w \end{bmatrix}; \quad \tilde{\mathbf{Q}}_{nc} = \begin{bmatrix} \mathbf{Q}^v \\ \mathbf{Q}^v_w \end{bmatrix}, \tag{7}$$

where, $\mathbf{q}$ is the (3×1) vector of generalized coordinates of the platform, (X,Y,ψ); $\mathbf{w}$ is the (8×1) wake oscillators variables vector; $\mathbf{M}$ is the (3×3) inertia matrix of the platform, including rigid body and added mass parcels[2]; $\mathbf{A}_w$ is the (8×8) matrix of inertial terms coupling the oscillators variables with the columns centers kinematics; $\mathbf{Q}^m$, $\mathbf{Q}^I$, $\mathbf{Q}^v$ are, respectively, the (3×1) vectors associated to the generalized mooring forces, centrifugal/Coriolis effects, and vortical viscous forces; $\mathbf{Q}_w^r$ and $\mathbf{Q}_w^v$ are the corresponding (8×1) vectors of restoring and damping effects related to the wake oscillators dynamics.

The wake oscillators model for each column k, $k=1,\ldots,N$, are written in the respective local in-line and transverse directions, (ξ,η), as presented below:

$$\begin{aligned}
&\ddot{w}_{\xi,k}+\varepsilon_\xi\omega_{s,k}(w_{\xi,k}^2-1)\dot{w}_{\xi,k}+4\omega_{s,k}^2 w_{\xi,k}=\frac{A_\xi}{D_k}a_{\xi,k},\\
&\ddot{w}_{\eta,k}+\varepsilon_\eta\omega_{s,k}(w_{\eta,k}^2-1)\dot{w}_{\eta,k}+\omega_{s,k}^2 w_{\eta,k}=\frac{A_\eta}{D_k}a_{\eta,k},
\end{aligned} \tag{8}$$

where $w_{\xi,k}$ and $w_{\eta,k}$ $(k=1,\ldots,N)$ are the hidden generalized coordinates that phenomenologically emulate the wake dynamics and its interaction with the structure; ε_ξ and ε_η are damping parameters; A_ξ and A_η are the inertial coupling parameters; D_k is the column diameter; $a_{\xi,k}$ and $a_{\eta,k}$ are the body-fixed components of the columns accelerations and $\omega_{s,k}=2\pi S_{t,k}\left(U_k/D_k\right)$ is the shedding frequency, with $S_{t,k}$ as the characteristic value of the Strouhal number for the case of low aspect ratio cylinders, and U_k is the relative velocity of the column center with respect to the flow. Notice that the in-line wake oscillator vibrates with twice the frequency corresponding to the crosswise one. This is a common *ad-hoc* assumption from experimental VIV observations, according to which the fundamental harmonic of hydrodynamic drag forces pulsates twice as fast as that of the lift forces. The coefficients $(\varepsilon_\xi,\varepsilon_\eta)$ and (A_ξ,A_η) have been calibrated from experiments (Rosetti, Fujarra, Nishimoto, & Ferreira, 2009; Rosetti, Gonçalves, Fujarra, & Nishimoto, 2011) and from CFD simulations (Postnikov, Pavlovskaia, & Wiercigroch, 2017). The appendix shows the ROM parameters.

3. RESULTS

The results are explored in terms of the motion amplitudes, force coefficients, as well as frequency and trajectories analysis. In general, both models provide good predictions concerning the experimentally observed behavior. The lock-in region is roughly the same, but there are some important differences in amplitudes of motion, in surge and sway. The CFD yields larger amplitudes whereas the ROM provides smaller ones, but still with satisfactory agreement to the experiments. There are some fundamental and important differences in the yaw amplitudes, which should be further investigated and analyzed. Furthermore, some local behavior differences can be spotted both in and outside of the lock-in region. And, due to its nature, the ROM simulations provide more organized trajectories, for which the well-known 8-figure shape can be seen for most of the reduced velocities; see Figure 7 and 8, (a)-(d). The CFD results, on the other hand, are characterized by more complex motions, Figure 7 and 8, (e)-(h), possibly due to particular phase differences among the hydrodynamic forces acting on each platform column, determined from pressure integration on the body, which cannot be captured by the phenomenological wake-oscillator model.

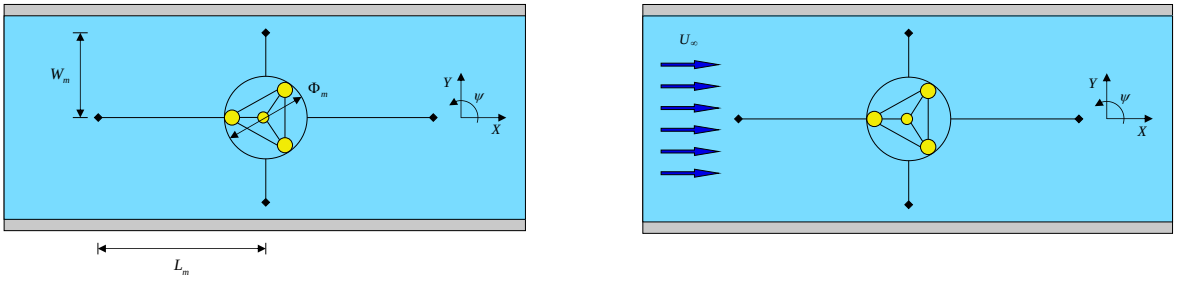

(a) (b)

Figure 6. Experiment sketch with the simplified mooring system. (a): tank sketch and mooring system geometry. (b): Incoming flow incidence at 0 degrees. Adapted from (de Oliveira, Pesce, Mendes, Orsino, & Franzini, 2020).

[2] The added mass matrix is determined from the potential flow theory, with no free surface effects. Both matrices, the body's and the added mass', are calculated in the body reference frame (ξ,η) and rotated to the inertial frame at each instant of time.

3.1 CFD results

By comparing the two-dimensional CFD results with the experimental data, we can observe that the VIM behavior was captured with a fair agreement; see Figure 9. The amplitudes are higher than obtained in the experiments, as expected, since the literature predicts higher drag and lift coefficients for simulations that neglect the three-dimensional effects, in this case related to the presence of heave plates, free-surface and free-edges. This explanation can be applied to both, surge and sway amplitudes, although for the first the differences obtained were significantly larger. For the transverse motion, while the lock-in range was fairly well captured, the peak amplitude in the CFD is observed at a considerably larger reduced velocity, possibly due to the coupling with in-line and yaw motions. Furthermore, there is a small jump in the transverse amplitude response between $V_r = 5.24$ and $V_r = 5.82$, which was not observed in the experimental results, but is accompanied by a peak in the lift coefficients.

Indeed, the most pronounced differences were obtained for the yaw amplitudes. Considerable differences in behavior are found when comparing the experimental and ROM with the CFD results. The latter captures a peak between $V_r = 5.24$ and $V_r = 9.89$ that is not reproduced in the others. The values obtained are also significantly higher, even after the peak. A possible explanation for this is that in the experiments the platform could move in heave, roll and pitch. Added to the heave plate presence, this could cause a significant difference in the flow field, altering the vortex emissions regime, that becomes more three-dimensional, affecting the coupling between the motions in the three degrees of freedom.

The mean drag coefficient results, as well as its RMS, were also reasonable, considering the simplified two-dimensional flow approach. The CFD predicted the experiment tendency, with a significant, but expected, translation to upper values. The absence of three-dimensionalities in the CFD simulations, again, is supposed to explain this behavior. The lift coefficients predicted by the CFD also accompanied the tendency of the experiments with larger values, but the peak was captured earlier, at $V_r = 5.24$, while in the experiments it was at $V_r = 7.5$. There is an abrupt drop in the CFD's lift coefficient after that peak, that is also not that pronounced in the experiments. This could have an influence on the discontinuity observed in the transverse amplitude results. The larger force coefficients obtained in the CFD also explain and are coherent with the larger displacement values observed in the trajectories (Figure 7), as well as with the larger platform's mean drifts (Figure 9 (h)), when compared to the ROM model.

3.2 ROM results

On the other hand, the ROM approach brings results that are in closer agreement with the experimental results, except for the yaw resonance regime, depicted at higher reduced velocities. Those facts were already observed and discussed in (de Oliveira, Pesce, Mendes, Orsino, & Franzini, 2020).

The ROM trajectories are qualitatively "well-behaved", Figure 7 (a)-(d), due to the dual synchronization hypothesis that is intrinsic to the wake oscillator model (Franzini & Bunzel, 2018). Also, the ROM produces a more realistic representation of the transverse oscillation amplitude with a maximum oscillations amplitude close to the one observed experimentally. The synchronization range obtained with the ROM also approximates the range observed in the experiments fairly well. Regarding the amplitude of the in-line oscillation, the ROM approximates the magnitude of the experimental results at the beginning of the crosswise oscillation synchronization range. Concerning the yaw motion, the ROM overestimated the amplitude significantly, showing a well-developed resonant response. Notice that although an increasing trend in the yaw motion may be seen from the small-scale experiments, there is no precise observation of such a resonant regime.

The hydrodynamic coefficients calculated with the ROM agree with the experiments. In particular, the mean drag estimated by the ROM fits well with the experiments. Conversely, the CFD produces a much rougher estimate, resulting in a most significant average drift displayed in the displacements series and in the mean horizontal displacement. Although the ROM is also restricted to motions on the horizontal plane, it is worth mentioning that some of the three-dimensional flow effects are contained in the Strouhal number parameter, through the shedding frequency $\omega_{s,k} = 2\pi S_{t,k}\left(U_k / D_k\right)$, that is present in the wake-oscillators equations, (7). In fact, the Strouhal number was taken from experimental results obtained with small draft cylinders, by (Gonçalves et al, 2015). For the external columns the adopted Strouhal number was $S_t = 0.145$ and for the internal one, $S_t = 0.150$ (de Oliveira, Pesce, Mendes, Orsino, & Franzini, 2020).

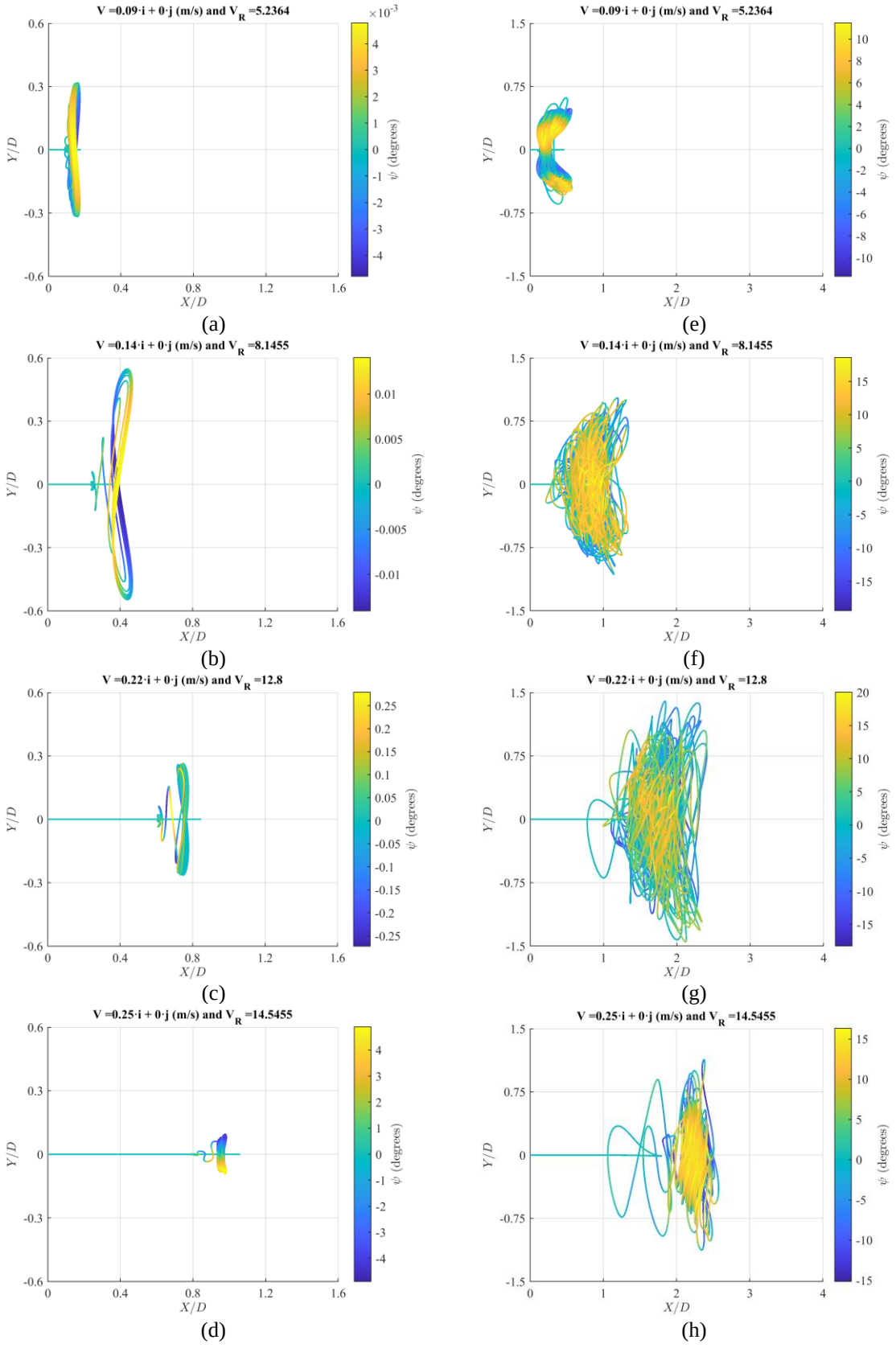

Figure 7. Trajectories of the FOWT's center on the horizontal plane (X is aligned with the current direction, in-line; Y is the transversal to it, cross). Yaw (in degrees) is scaled as in the colored bar. (a)–(d): ROM; (e)–(h): CFD. (a), (e): V_R = 5.24; (b), (f): V_R = 8.15; (c), (g): V_R = 12.8; (d), (h): V_R = 14.55.

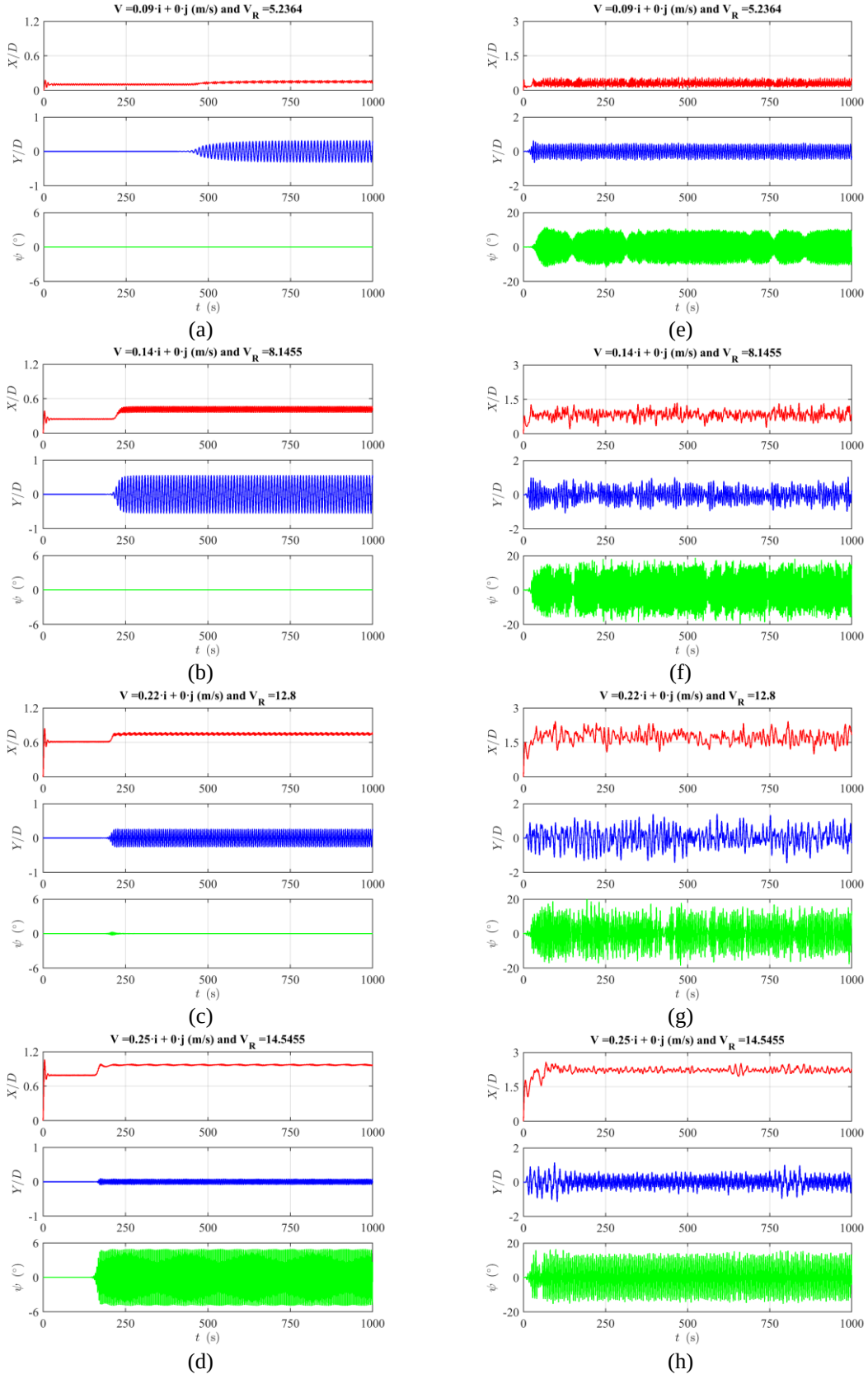

Figure 8. Time series of the FOWT's displacements on the horizontal plane (X is aligned with the current direction, in-line; Y is the transversal to it, cross). (a)–(d): ROM; (e)–(h): CFD. (a), (e): V_R = 5.24; (b), (f): V_R = 8.15; (c), (g): V_R = 12.8; (d), (h): V_R = 14.55.

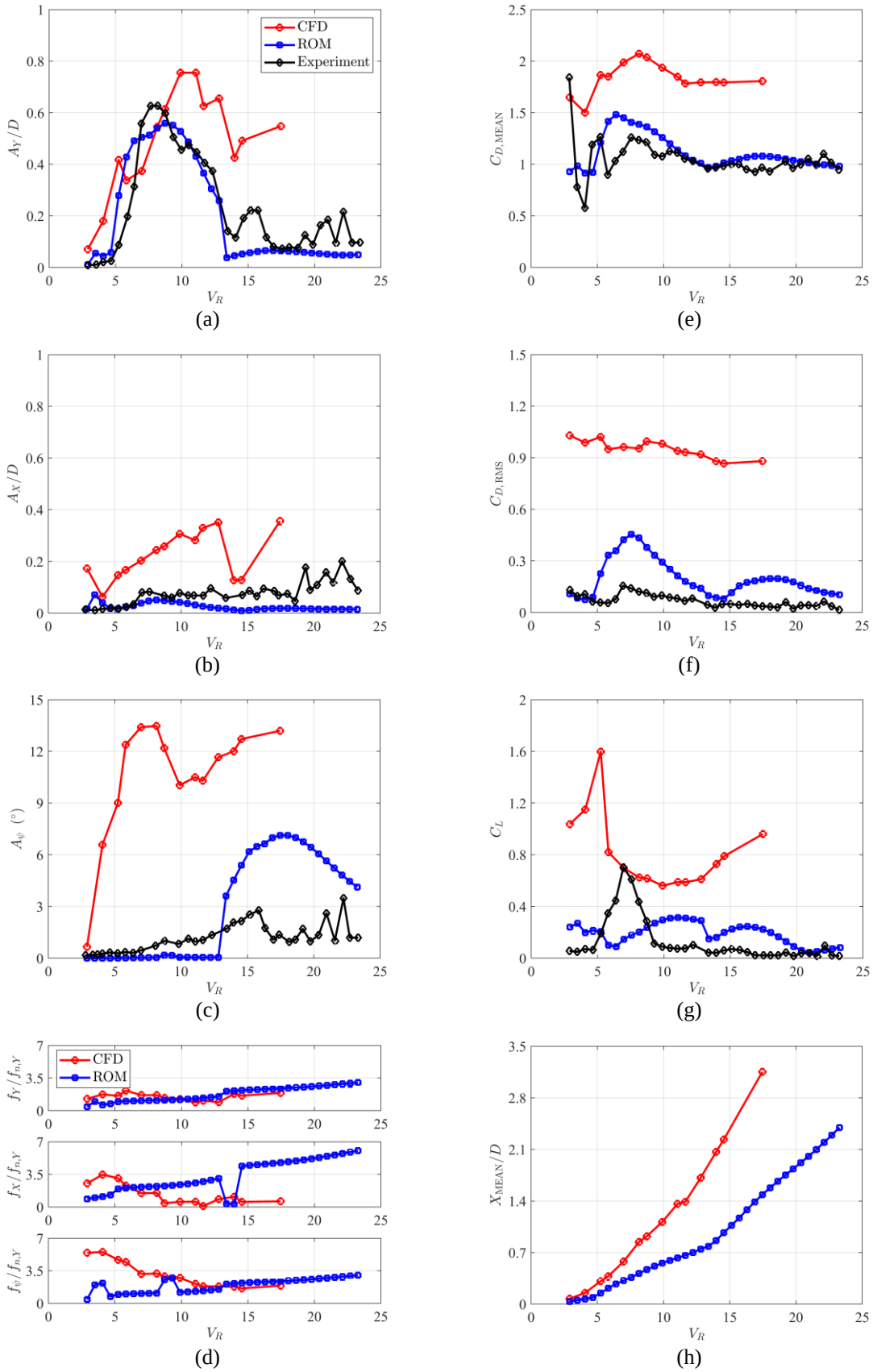

Figure 9. Comparison with experimental results. (a): Cross flow amplitude; (b): In-line amplitude; (c): Yaw amplitude; (d): Dominant nondimensional oscillation frequencies; (e): Mean drag coefficient; (f): RMS of the Drag coefficient; (g): Lift coefficient; (h): Mean in-line drift.

4. CONCLUSIONS

The CFD simulations captured good tendencies of the VIM response. The absence of three-dimensional effects in the CFD model explains the higher values obtained. Some important differences were observed, though, especially in the yaw motion. The interaction between the vortex emissions on each column could affect the yaw frequency and amplitudes, making the CFD results to be quite different than the ones obtained by the ROM model, and possibly affecting the CFD's sway and surge response results. The presence, *in the experiment*, of the other 3 degrees of freedom, is also an important factor to be considered, as the platform's inclination in pitch can considerably affect the flow and the coupling between the motions, changing the VIM response. Further work should explore 3D CFD simulations.

On the other hand, despite some relatively strong simplifying assumptions adopted in the mathematical modelling of such a complex phenomenon, the results obtained with the ROM are in better agreement with the experiments. This is thought to be due to the 3D effects incorporated into the ROM via the Strouhal number of the small aspect ratio columns obtained experimentally. Other important feature associated with the ROM is very low computational burden compared to the CFD model. Further improvements in the ROM should consider the effects of wake interferences between columns, dependent on the spacing between them. Parametric sensitivity studies may be planned, as well.

5. ACKNOWLEDGEMENTS

This work was developed as part of the R&D project conducted by Petrobras, and the University of São Paulo entitled "Research and Development on Deep Water Floating Offshore Wind Turbines'" (agreement Petrobras #5900.0112605.19.9, under the levy regulation of the Brazilian National Petroleum Agency (Agência Nacional do Petróleo, ANP). B. S. Carmo and C. Pesce thank the Brazilian National Council for Scientific and Technological Development (CNPq) for the research grants, numbers 314221/2021-2 and 307995/2022-4, respectively.

6. REFERENCES

de Oliveira, É. L., Pesce, C. P., Mendes, B., Orsino, R. M., & Franzini, G. R. (2020). A Reduced Order Mathematical Model for the Currend-Induced Motion of a Floating Offshore Wind Turbine. *Proceedings of ASME 2020 - 3rd International Offshore Wind Technical Conference.* Boston, MA, USA: ASME.

EPE, E. d. (2022). *www.epe.gov.br*. Retrieved from https://www.epe.gov.br/pt/abcdenergia/matriz-energetica-e-eletrica

Franzini, G. R., & Bunzel, L. O. (2018). A numerical investigation on piezoelectric energy harvesting from Vortex-Induced Vibrations with one and two degrees of freedom. *Journal of Fluids and Structures*.

Gonçalves, R. T. (2019). *Private communication with the authors*.

Gonçalves, R. T., Chame, M. E., Silva, L. S., Koop, A., Hirabayashi, S., & Suzuki, H. (2019). EXPERIMENTAL STUDY ON FLOW-INDUCED MOTIONS (FIM) OF A FLOATING OFFSHORE WIND TURBINE SEMI-SUBMERSIBLE TYPE (OC4 PHASE II FLOATER). *ASME 2019 2nd International Offshore Wind Technical Conference, IOWTC2019.* St. Julian's, Malta.

Gonçalves, R. T., Franzini, G. R., Rosetti, G. F., Meneghini, J. R., & Fujarra, A. L. (2015). Flow around circular cylinders with very low aspect ratio. *J Fluids and Structures, 54*, pp. 122-141.

Menter, F. R. (1994). Two-equation eddy-viscosity turbulence models for engineering applications . 305-316.

Pesce, C. P., Amaral, G. A., & Franzini, G. R. (2018). Mooring System Stiffness: A General Analytical Formulation With an Application to Floating Offshore Wind Turbines. *Proceedings of the ASME 2018 1st International Offshore Wind Technical Conference.* San Francisco, CA, USA: ASME.

Postnikov, A., Pavlovskaia, E., & Wiercigroch, M. (2017). 2-dof CFD calibrated wake oscillator model to investigate vortex-induced vibrations. *Int J of Mech Sciences 127*, pp. 176-190.

Rosetti, G. F., Fujarra, A. L., Nishimoto, K., & Ferreira, M. D. (2009). A phenomenological model for vortex-induced motions of the monocolumn platform and comparison with experiments. *ASME 2009 28th Int Conf on Ocean, Offshore and Arctic Engineering.*

Rosetti, G. F., Gonçalves, R. T., Fujarra, A. L., & Nishimoto, K. (2011). Parametric Analysis of a Phenomenological Model for Vortex-Induced Motions of Monocolumn Platforms. *J of the Brazilian Soc of Mechanical Sciences and Engineering, 33 (6)*, pp. 139-146.

Scopel, A. X. (2022). Numerical analysis of vortex-induced motions on floating offshore wind turbine platforms. São Paulo, SP, Brazil: Escola Politécnica da Universidade de São Paulo.

Weller, H., Tabor, G., Jasak, H., & Fureby, C. (1998). A Tensorial Approach to Computational Continuum Mechanics Using Object-Oriented Techniques. *Computers in Physics*, 620-631.

7. RESPONSIBILITY NOTICE

The authors are the only responsible for the printed material included in this paper.

8. APPENDIX

The parameters used in the ROM simulations are found in Tables 2-6.

Table 2. OC4 scaled model parameters; (Gonçalves et al., 2019).

Parameters	Values
Draught, H (m)	0.275
Arc radius, R (m)	0.490
Columns centers' radius, r (m)	0.397
Diameters, $\{D_1, D_2, D_3, D_4\}$ (m)	{0.165, 0.165, 0.165, 0.090}
Platform's mass matrix, $\mathbf{M}_p$ (kg, kg, kgm²)	diag{36.70, 36.70, 4.00}
Added mass tensor, $\hat{\mathbf{M}}_a$ (kg, kg, kgm²)	diag{21.72, 22.13, 4.39}
Density of water, ρ (kg/m³)	1000

Table 3. Mooring system parameters; (Gonçalves et al., 2019; Gonçalves, 2019).

Parameters	Values
Towing car dimensions, $\{W_m, L_m, \Phi_m\}$ (m)	{1.59, 2.40, 0.98}
Natural lengths $\{l_{n_1}, l_{n_2}, l_{n_3}, l_{n_4}\}$ (m)	{0.80, 0.425, 0.80, 0.425}
Spring constants $\{k_1, k_2, k_3, k_4\}$ (N/m)	{7.46, 9.42, 7.46, 9.42}

Table 4. Wake-oscillators parameters; (Rosetti, Fujarra, Nishimoto, & Ferreira, 2009; Gonçalves, Franzini, Rosetti, Meneghini, & Fujarra, 2015).

Parameters	Values
$\{A_\xi, A_\eta\}$	{12, 6}
$\{\varepsilon_\xi, \varepsilon_\eta\}$	{0.30, 0.15}
$\{C_{D0}, C_{L0}, C_{D0}^f, K\}$	{0.70, 0.30, 0.10, 0.05}
Strouhal numbers for each column, $\{S_{t_1}, S_{t_2}, S_{t_3}, S_{t_4}\}$	{0.145, 0.145, 0.145, 0.150}

Table 5. Mass and stiffness matrices at the trivial equilibrium position; (Gonçalves et al., 2019; Gonçalves, 2019).

Incidence	0°, 180°	90°
Mass matrix, $\mathbf{M}$ (kg, kg, kgm²)	diag{58.42, 58.83, 8.39}	diag{58.83, 58.42, 8.39}
Mooring stiffness matrix, $\mathbf{K}$ (N/m, N/m, Nm)	diag{26.48, 27.46, 19.22}	diag{26.48, 27.46, 19.22}

Table 6. Natural periods at the trivial equilibrium position; (Gonçalves et al., 2019; Gonçalves, 2019).

	Experiment		ROM	
Incidence	0°, 180°	90°	0°, 180°	90°
DOF	T_n (s)	T_n (s)	T_n (s)	T_n (s)
X	9.40	9.40	9.33	9.36
Y	9.60	9.70	9.20	9.16
Ψ	4.20	4.20	4.15	4.15